Research Article | Vol. 26, No. 4 | 19 Feb 2018 | OPTICS EXPRESS 4448
Optics EXPRESS

Broadband and efficient adiabatic three-wave-mixing in a temperature-controlled bulk crystal

ANDREY MARKOV,[1] ANNA MAZHOROVA,[1] HOLGER BREITENBORN,[1] ANDREW BRUHACS,[1] MATTEO CLERICI,[2] DANIELE MODOTTO,[3] OTTAVIA JEDRKIEWICZ,[4] PAOLO DI TRAPANI,[5] ARKADY MAJOR,[6] FRANÇOIS VIDAL,[1] AND ROBERTO MORANDOTTI[1,7,8,*]

[1]*INRS-EMT, Varennes, Québec J3X 1S2, Canada*
[2]*School of Engineering, University of Glasgow, Glasgow, G12 8LT, UK*
[3]*Dipartimento di Ingegneria dell'Informazione, Università di Brescia, via Branze 38, 25123 Brescia, Italy*
[4]*CNR and CNISM Udr Como, Via Valleggio 11, 22100 Como, Italy*
[5]*University of Insubria and CNISM Udr Como, Via Valleggio 11, 22100, Como, Italy*
[6]*Department of Electrical and Computer Engineering, University of Manitoba, Winnipeg, Manitoba, R3T 5V6, Canada*
[7]*National Research University of Information Technologies, Mechanics and Optics, 199034 St. Petersburg, Russia*
[8]*Institute of Fundamental and Frontier Sciences, University of Electronic Science and Technology of China, Chengdu 610054, Sichuan, China*
[*]*morandotti@emt.inrs.ca*

Abstract: Nonlinear interactions are commonly used to access to wavelengths not covered by standard laser systems. In particular, optical parametric amplification (OPA) is a powerful technique to produce broadly tunable light. However, common implementations of OPA suffer from a well-known trade-off, either achieving high efficiency for narrow spectra or inefficient conversion over a broad bandwidth. This shortcoming can be addressed using adiabatic processes. Here, we demonstrate a novel technique towards this direction, based on a temperature-controlled phase mismatch between the interacting waves. Using this approach, we demonstrate, by tailoring the temperature profile, an increase in conversion efficiency by 21%, reaching a maximum of 57%, while simultaneously expanding the bandwidth to over 300 nm. Our technique can readily enhance the performances of current OPA systems.

OCIS codes: (190.4223) Nonlinear wave mixing; (190.4410) Nonlinear optics, parametric processes; (190.4970) Parametric oscillators and amplifiers; (260.3060) Infrared.

References and links

1. M. Fejer, G. Magel, D. Jundt, and R. Byer, "Quasi-phase-matched second harmonic generation: tuning and tolerances," IEEE J. Quantum Electron. **28**(11), 2631–2654 (1992).
2. Y. Nabekawa and K. Midorikawa, "Broadband sum frequency mixing using noncollinear angularly dispersed geometry for indirect phase control of sub-20-femtosecond UV pulses," Opt. Express **11**(4), 324–338 (2003).
3. N. E. Yu, J. H. Ro, M. Cha, S. Kurimura, and T. Taira, "Broadband quasi-phase-matched second-harmonic generation in MgO-doped periodically poled $LiNbO_3$ at the communications band," Opt. Lett. **27**(12), 1046–1048 (2002).
4. H.-H. Lim, O. Prakash, B.-J. Kim, K. Pandiyan, M. Cha, and B. K. Rhee, "Ultra-broadband optical parametric generation and simultaneous RGB generation in periodically poled lithium niobate," Opt. Express **15**(26), 18294–18299 (2007).
5. O.-Y. Jeon, M.-J. Jin, H.-H. Lim, B.-J. Kim, and M. Cha, "Broadband optical parametric generation in the telecommunication band and simultaneous RGB generation by quasi-phase-matched parametric conversion processes," J. Korean Phys. Soc. **49**, S589–S591 (2006).
6. B. E. Schmidt, N. Thiré, M. Boivin, A. Laramée, F. Poitras, G. Lebrun, T. Ozaki, H. Ibrahim, and F. Légaré, "Frequency domain optical parametric amplification," Nat. Commun. **5**, 3643 (2014).

#309238 https://doi.org/10.1364/OE.26.004448
Journal © 2018 Received 16 Oct 2017; revised 2 Feb 2018; accepted 3 Feb 2018; published 12 Feb 2018

Optics EXPRESS

7. B. E. Schmidt, P. Lassonde, G. Ernotte, M. Clerici, R. Morandotti, H. Ibrahim, and F. Légaré, "Decoupling Frequencies, Amplitudes and Phases in Nonlinear Optics," Sci. Rep. **7**(1), 7861 (2017).
8. V. Veksler, "A new method of acceleration of relativistic particles," J. Phys. USSR **9**, 153 (1945).
9. E. M. McMillan, "The synchrotron - a proposed high energy particle accelerator," Phys. Rev. **68**(5-6), 143–144 (1945).
10. B. Meerson and L. Friedland, "Strong autoresonance excitation of Rydberg atoms: The Rydberg accelerator," Phys. Rev. A **41**(9), 5233–5236 (1990).
11. W. K. Liu, B. Wu, and J. M. Yuan, "Nonlinear dynamics of chirped pulse excitation and dissociation of diatomic molecules," Phys. Rev. Lett. **75**(7), 1292–1295 (1995).
12. G. Marcus, L. Friedland, and A. Zigler, "From quantum ladder climbing to classical autoresonance," Phys. Rev. A **69**(1), 013407 (2004).
13. H. Maeda, J. Nunkaew, and T. F. Gallagher, "Classical phase locking in adiabatic rapid passage," Phys. Rev. A **75**(5), 053417 (2007).
14. G. Manfredi and P. A. Hervieux, "Autoresonant control of the many-electron dynamics in nonparabolic quantum wells," Appl. Phys. Lett. **91**(6), 061108 (2007).
15. L. A. Kalyakin, M. A. Shamsutdinov, R. N. Garifullin, and R. K. Salimov, "Autoresonance parametric excitation of localized oscillations of magnetization in a ferromagnet by an AC field of a variable frequency," Phys. Met. Metallogr. **104**(2), 107–120 (2007).
16. M. A. Shamsutdinov, L. A. Kalyakin, and A. T. Kharisov, "Autoresonance in a ferromagnetic film," Tech. Phys. **55**(6), 860–865 (2010).
17. S. V. Batalov and A. G. Shagalov, "Autoresonance control of a magnetization soliton," Phys. Met. Metallogr. **109**(1), 1–6 (2010).
18. O. Naaman, J. Aumentado, L. Friedland, J. S. Wurtele, and I. Siddiqi, "Phase-locking transition in a chirped superconducting Josephson resonator," Phys. Rev. Lett. **101**(11), 117005 (2008).
19. G. A. Brucker and G. J. Rathbone, "Autoresonant Trap Mass Spectrometry (ART MS) for remote sensing applications," Int. J. Mass Spectr. **295**(3), 133–137 (2010).
20. A. V. Ermakov and B. J. Hinch, "An electrostatic autoresonant ion trap mass spectrometer," Rev. Sci. Instrum. **81**(1), 013107 (2010).
21. R. R. Lindberg, A. E. Charman, J. S. Wurtele, and L. Friedland, "Robust autoresonant excitation in the plasma beat-wave accelerator," Phys. Rev. Lett. **93**(5), 055001 (2004).
22. O. Yaakobi, L. Friedland, R. Lindberg, A. Charman, G. Penn, and J. Wurtele, "Spatially autoresonant stimulated Raman scattering in nonuniform plasmas," Phys. Plasmas **15**(3), 032105 (2008).
23. A. Barak, Y. Lamhot, L. Friedland, and M. Segev, "Autoresonant dynamics of optical guided waves," Phys. Rev. Lett. **103**(12), 123901 (2009).
24. O. Yaakobi, M. Clerici, L. Caspani, F. Vidal, and R. Morandotti, "Complete pump depletion by autoresonant second harmonic generation in a nonuniform medium," J. Opt. Soc. Am. B **30**(6), 1637–1642 (2013).
25. O. Yaakobi, L. Caspani, M. Clerici, F. Vidal, and R. Morandotti, "Complete energy conversion by autoresonant three-wave mixing in nonuniform media," Opt. Express **21**(2), 1623–1632 (2013).
26. H. Suchowski, D. Oron, A. Arie, and Y. Silberberg, "Geometrical representation of sum frequency generation and adiabatic frequency conversion," Phys. Rev. A **78**(6), 063821 (2008).
27. A. Leshem, G. Meshulam, G. Porat, and A. Arie, "Adiabatic second-harmonic generation," Opt. Lett. **41**(6), 1229–1232 (2016).
28. A. Dahan, A. Levanon, M. Katz, and H. Suchowski, "Ultrafast adiabatic second harmonic generation," J. Phys. Condens. Matter **29**(8), 084004 (2017).
29. H. Suchowski, V. Prabhudesai, D. Oron, A. Arie, and Y. Silberberg, "Robust adiabatic sum frequency conversion," Opt. Express **17**(15), 12731–12740 (2009).
30. C. Heese, C. R. Phillips, L. Gallmann, M. M. Fejer, and U. Keller, "Ultrabroadband, highly flexible amplifier for ultrashort midinfrared laser pulses based on aperiodically poled Mg:$LiNbO_3$," Opt. Lett. **35**(14), 2340–2342 (2010).
31. C. Heese, C. R. Phillips, B. W. Mayer, L. Gallmann, M. M. Fejer, and U. Keller, "75 MW few-cycle mid-infrared pulses from a collinear apodized APPLN-based OPCPA," Opt. Express **20**(24), 26888–26894 (2012).
32. C. R. Phillips, C. Langrock, D. Chang, Y. W. Lin, L. Gallmann, and M. M. Fejer, "Apodization of chirped quasi-phasematching devices," J. Opt. Soc. Am. B **30**(6), 1551–1568 (2013).
33. C. R. Phillips, B. W. Mayer, L. Gallmann, M. M. Fejer, and U. Keller, "Design constraints of optical parametric chirped pulse amplification based on chirped quasi-phase-matching gratings," Opt. Express **22**(8), 9627–9658 (2014).
34. P. Krogen, H. Suchowski, H. Liang, N. Flemens, K.-H. Hong, F. X. Kärtner, and J. Moses, "Generation and multi-octave shaping of mid-infrared intense single-cycle pulses," Nat. Photonics **11**(4), 222–226 (2017).
35. G. Porat and A. Arie, "Efficient, broadband, and robust frequency conversion by fully nonlinear adiabatic three-wave mixing," J. Opt. Soc. Am. B **30**(5), 1342–1351 (2013).
36. R. A. Haas, "Influence of a constant temperature gradient on the spectral-bandwidth of second-harmonic generation in nonlinear crystals," Opt. Commun. **113**(4-6), 523–529 (1995).
37. K. Regelskis, J. Želudevičius, N. Gavrilin, and G. Račiukaitis, "Efficient second-harmonic generation of a broadband radiation by control of the temperature distribution along a nonlinear crystal," Opt. Express **20**(27), 28544–28556 (2012).

Optics EXPRESS

38. Y. L. Lee, Y.-C. Noh, C. Jung, T. Yu, D.-K. Ko, and J. Lee, "Broadening of the second-harmonic phase-matching bandwidth in a temperature-gradient-controlled periodically poled Ti:$LiNbO_3$ channel waveguide," Opt. Express **11**(22), 2813–2819 (2003).
39. K. K. Y. Wong, M. Marhic, and L. Kazovsky, "Temperature control of the gain spectrum of fiber optical parametric amplifiers," Opt. Express **13**(12), 4666–4673 (2005).
40. O. Yaakobi and L. Friedland, "Autoresonant four-wave mixing in optical fibers," Phys. Rev. A **82**(2), 023820 (2010).
41. R. Boyd, Nonlinear Optics (Academic, 2008).
42. C. R. Menyuk, R. Schiek, and L. Torner, "Solitary waves due to $x^{(2)}$:$x^{(2)}$cascading," J. Opt. Soc. Am. B **11**(12), 2434–2443 (1994).
43. A. V. Buryak, P. Di Trapani, D. V. Skryabin, and S. Trillo, "Optical solitons due to quadratic nonlinearities: from basic physics to futuristic applications," Phys. Rep. **370**(2), 63–235 (2002).
44. K. Kato, "Temperature-tuned 90° phase-matching properties of LiB_3O_5," IEEE J. Quantum Electron. **30**(12), 2950–2952 (1994).

1. Introduction

Three-wave-mixing (TWM) in second-order nonlinear optical crystals is a powerful technique to produce broadly tunable high energy ultra-short pulses. In particular, TWM has been widely exploited for optical parametric amplification (OPA), for which it enables conversion to wavelength regions inaccessible to standard laser systems. In order to produce very short pulses, the generation of ultra-broad spectra is essential. However, the output pulse duration in parametric processes is typically limited by the spectral acceptance of the nonlinear medium.

Standard techniques offer high efficiency operation for narrowband spectra or inefficient performance over broad bandwidths. Moreover, energy coupling between the waves interacting in a uniform medium leads to a periodic forward- and back-conversion along the propagation axis. Even if the wave vectors of the interacting waves are nearly-perfectly matched, conversion may reach its maximum value only at specific positions along this axis. Such periodicity causes the efficiency to be very sensitive to system parameters, e.g. interaction length, pump power, wavelengths, temperature, etc.

Several methods have been proposed to resolve these issues and increase the TWM efficiency over a broad bandwidth, including quasi-phase-matching with chirped gratings [1], non-collinear angularly dispersed geometry [2], or group-velocity matching techniques [3–5]. More complex frequency conversion schemes deploy multiple crystals. Among those, a 600 nm bandwidth amplification with 10-14% efficiency was achieved using frequency domain OPA [6,7]. However, these setups are typically bulky and require complex alignment.

An adiabatic TWM process has the potential to achieve an efficient broadband response, taking advantage of the autoresonance effect. Autoresonance is a unique property of nonlinear systems to remain in resonance with driving oscillations, if the parameters of the system vary gradually in time and/or space. Autoresonance techniques were first exploited in relativistic particle accelerators [8,9], and found, over the last decades, widespread applications in the excitation and control of various and diverse nonlinear phenomena (e.g. in atomic, molecular and semiconductors physics [10–14], ferromagnetism [15–17], Josephson junctions [18], ion mass spectrometry [19,20], and plasma physics [21,22]). The first experimental demonstration of autoresonance in optics was carried out using a mixing process of two linearly-coupled waves [23].

Building upon this effect, adiabatic TWM in a nonlinear crystal can result in high conversion efficiencies over a remarkable bandwidth [24,25]. For this process to occur, the phase mismatch (Δk) between the mixed waves is slowly tuned from $\Delta k < 0$ to $\Delta k > 0$ (or vice versa) along the propagation axis, allowing the adiabatic conversion to adapt to these (slow) changes [26]. Herein, the conversion of different frequency components occurs at specific positions along the nonlinear crystal, where $\Delta k \approx 0$ for a given frequency component, thus resulting in a broadband, efficient operation over the whole crystal length. For a weak variance of the phase mismatch, the efficiency of the energy conversion between the interacting waves can reach almost 100%. A system under autoresonance conditions exhibits

Optics EXPRESS

a monotonic change in energy distribution between the interacting waves. Moreover, the variation of phase mismatch along the propagation direction renders the final conversion efficiency less sensitive to the system parameters, making the proposed approach robust against changes in the working environment [27,28].

So far, adiabatic conversion has been mainly demonstrated in periodically poled (PP) materials, showing high efficiency and broad bandwidth. For example, sum-frequency generation in PP-KTP crystals with chirped gratings exhibits over 50% efficiency and 170 nm bandwidth in the 1400-1700 nm wavelength range [26,29]. By extending the signal wavelength to 3-4 μm, it is possible to achieve an OPA bandwidth of 800 nm [30,31]. This value can be further improved by means of apodized gratings [32,33]. Furthermore, the adiabatic frequency conversion in a larger-than-octave-spanning range has allowed for the generation of nearly single cycle mid-IR pulses [34]. As well, virtually fully-efficient sum- and difference- frequency generation has been theoretically predicted [35].

Nevertheless, PP materials suffer from a number of technical issues. They require difficult fabrication with sub-micron resolution. Moreover, lower photorefractive damage thresholds compared to their bulk counterparts, as well as smaller aperture sizes (~1 mm) of the available PP crystals, make them unsuitable for high power operation. More importantly, the phase-matching properties of the PP crystals are not readily reconfigurable, i.e. the amplification bandwidth is primarily determined by the poling period of the crystal. Thus, the same crystal cannot be reconfigured to amplify different wavelength regions. All of these limitations, however, can be overcome by using bulk nonlinear optical crystals. One of the most promising approaches is to implement a temperature gradient along the direction of light propagation [36]. This has been experimentally shown in a nonlinear lithium triborate (LiB_3O_5 – LBO) crystal and has led to improved conversion efficiency in second harmonic generation over a narrow bandwidth [37]. This technique has also been applied to broaden the phase-matching bandwidth in a periodically-poled channel waveguide up to 13 nm [38], as well as to shift the gain wavelength position in a fiber OPA [39].

Here, we present an adiabatic wavelength conversion approach based on a non-uniform temperature distribution, and study broadband OPA in bulk nonlinear crystals, both experimentally and through a series of comprehensive simulations. For the first time, to the best of our knowledge, the temperature control technique is applied to simultaneously increase the bandwidth and the efficiency of the nonlinear process. In particular, we have examined how various applied temperature profiles affect the conversion efficiency. Finally, we have optimized the temperature distribution to provide efficient broadband TWM in the 1200-1550 nm wavelength range, in turn demonstrating a conversion efficiency of about 50% over more than a 250-nm bandwidth. Besides its fundamental interest, the introduced technique of controlling the phase-matching by applying a temperature gradient along nonlinear bulk crystals can find applications in a new generation of OPAs, since it does not require any complex fabrication or alignment techniques. Furthermore, it can be easily used to expand the capabilities of existing OPA setups. This simple approach allows for on-the-fly reconfigurability of the operating wavelengths since the same crystal can be used to meet phase-matching conditions over a wide spectral range.

2. Theory

Current autoresonant theory provides analytical expressions for the amplitudes of the propagating waves and delivers the phase-matching conditions that are required for stable operation and hence efficient TWM over a wide wavelength range [25,40].

The theory is expressed by a set of equations that describes, in a plane wave approximation, the spatial evolution of the pump, signal, and idler waves in a non-uniform crystal, assuming that the group velocity dispersion is negligible. The refractive indices, the wave vectors, and their mismatch are functions of the position z along the crystal. These equations are generic and do not depend on the physical origin of the non-uniformity,

Optics EXPRESS

although they can also provide the stability/efficiency conditions for the specific case of temperature induced non-uniformity. The system of equations outlining the slow envelopes of the three interacting waves can be written as [41]:

$$\begin{aligned} & j\frac{\partial A_{1,2}}{\partial z}+\frac{\omega_{1,2}}{n_{1,2}c}\chi_{eff}A_{2,1}^{*}A_{3}\exp\left\{+j\int_{0}^{z}\Delta k(\zeta)d\zeta\right\}=0 \\ & j\frac{\partial A_{3}}{\partial z}+\frac{\omega_{3}}{n_{3}c}\chi_{eff}A_{1}A_{2}\exp\left\{-j\int_{0}^{z}\Delta k(\zeta)d\zeta\right\}=0 \\ & \Delta k(z)=k_{3}(z)-k_{1}(z)-k_{2}(\mathrm{z}),\quad k_{1,2,3}(z)=\frac{2\pi}{\lambda_{1,2,3}}n_{1,2,3}(z) \end{aligned} \tag{1},$$

where $A_j(z)$ is the envelope of the electric field of the j-th wave; j is equal to 1, 2 and 3 for the idler, signal, and pump waves, respectively; $d_{eff}=\chi_{eff}/2$ is the quadratic nonlinear coefficient of the optical medium; k_j is the j-th wave vector, and $\Delta k(z)$ is the phase-mismatch. The coupling coefficients can be defined as $\eta_j=\chi_{eff}\omega_j^2/(k_jc^2)$. To obtain an analytical solution, the phase mismatch must be considered as a linear function of the position $\Delta k=\alpha(z-z_*)/l^2=\alpha\cdot\xi/l$, where α is the non-uniformity rate coefficient; z_* corresponds to the position at which perfect phase-matching ($\Delta k=0$) occurs, and $\xi=(z-z_*)/l$ is the shifted normalized coordinate, where:

$$l=1/\left[\left(\eta_1\eta_2\right)^{1/2}\left|A_{3,0}\right|\right]=\left[\left(\frac{c\varepsilon_0}{8\pi^2}\right)\cdot\frac{n_{1,avg}n_{2,avg}n_{3,0}\lambda_1\lambda_2}{d_{eff}^2I_{3,0}}\right]^{1/2} \tag{2}$$

is the length normalization parameter, and $A_{3,0}$ is the pump electric field at the input [25].

Starting with a sufficiently large negative value of $\Delta k\cdot l=|\alpha|\cdot\xi$, we guarantee the phase-locking (constant phase difference) of the interacting waves. If the pump wave intensity is much higher than both signal and idler, the system dynamics can be divided into two stages. In the first stage (typically, when $|\alpha|\xi<-2$) the energy of the pump is considered constant, the variation of the signal intensity is neglected, and only the evolution of the idler wave is taken into account. At this stage, the initial phase-locking is being established. At the point where $|\alpha|\xi=-2$, the amplitudes of the idler and signal waves become comparable to each other. In the second stage of the autoresonance process ($|\alpha|\xi>-2$), pump depletion must be taken into account; phase-locking is preserved and the pump energy is depleted with a monotonic increase in the energy of the signal and idler waves until almost complete (90%) depletion is achieved at $|\alpha|\xi=2$ (see [25] and [40] for additional details on different stages of the autoresonant process).

Since the most prominent autoresonant dynamics occur between $|\alpha|\xi=-2$ and $|\alpha|\xi=2$, the system parameter variations must include the $-2<|\alpha|\xi<2$ region to allow efficient autoresonant TWM, or equivalently it requires relatively high values of the phase mismatch at the crystal extremities

$$|\Delta k_{ini}|,|\Delta k_{fin}|>\frac{2}{l} \tag{3}$$

Optics EXPRESS

This guarantees initial phase-locking and a subsequent transfer of almost all of the pump wave energy into the signal and idler waves. However, to obtain stable phase-locked dynamics everywhere along the propagation, it is required that $|\alpha| \ll 1$. This condition can be rewritten as:

$$\left|\Delta k_{fin} - \Delta k_{ini}\right| \ll \frac{L}{l^2} \tag{4},$$

where L is the length of the crystal. This set of conditions is only loosely satisfied for commonly used nonlinear crystals and for this reason experiments cannot show the almost complete pump depletion demonstrated in earlier theoretical papers [25]. Improvements for an efficient autoresonant mixing process can therefore be achieved either by extending the crystal length (impractical as it introduces a larger temporal walk-off between the pulses), increasing the photon flux (limited by the crystal's damage threshold), and/or deploying a crystal with a larger effective nonlinear susceptibility.

3. Simulations

The autoresonance theory correctly predicts a wider wavelength range of efficient conversion in non-uniform crystals than that achievable in a uniform medium. However, it imposes multiple restrictions on the interacting wave intensity and on the rate of non-uniformity in the medium [Eqs. (3) and (4)]. For example, the conversion of femtosecond pulses requires an extremely large phase-matching bandwidth (over 300 nm for 10 fs pulses centered at 800 nm) and therefore a very high non-uniformity in the crystal, thus preventing the autoresonance theory from accurately predicting the efficiency of the process. To achieve a more accurate physical picture, a comprehensive numerical analysis of the wave-mixing phenomenon is required, which should also include diffraction to accurately model focused beams, and group velocity dispersion to account for the temporal walk-off of the interacting waves.

Equation set (1) must be replaced by the following formulae for the slowly-varying envelopes $A_j(x,y,z,t)$, which not only depend on the propagation coordinate z, but also on the transverse spatial coordinates x, y and on the time t [42,43]:

$$\begin{aligned}
&j\frac{\partial A_{1,2}}{\partial z} + \frac{1}{2k_{1,2}}\frac{\partial^2 A_{1,2}}{\partial x^2} + \frac{1}{2k_{1,2}}\frac{\partial^2 A_{1,2}}{\partial y^2} + j\frac{1}{v_{1,2}}\frac{\partial A_{1,2}}{\partial t} \\
&+ \frac{\omega_{1,2}}{n_{1,2}c}\chi_{eff} A_{2,1}^* A_3 \exp\left\{+j\int_0^z \Delta k(\zeta)d\zeta\right\} = 0 \\
&j\frac{\partial A_3}{\partial z} + \frac{1}{2k_3}\frac{\partial^2 A_3}{\partial x^2} + \frac{1}{2k_3}\frac{\partial^2 A_3}{\partial y^2} + j\frac{1}{v_3}\frac{\partial A_3}{\partial t} \\
&+ \frac{\omega_3}{n_3 c}\chi_{eff} A_1 A_2 \exp\left\{-j\int_0^z \Delta k(\zeta)d\zeta\right\} = 0 \\
&\Delta k = k_3 - k_1 - k_2, \quad k_{1,2,3} = \frac{2\pi}{\lambda_{1,2,3}} n_{1,2,3}
\end{aligned} \tag{5}.$$

Here, the second order spatial derivatives model diffraction, whereas the effect of the different group velocities at the idler (v_1), signal (v_2) and pump (v_3) wavelengths is accounted for by the time partial derivatives. The refractive indices (and thus Δk) depend on the temperature [44], which in our scheme is a function of z. Equation set (5) is numerically solved by means of a standard split-step method.

The conversion efficiency is defined as:

Optics EXPRESS

$$\eta = \frac{W_{s+i,\,pump} - W_{s,\,\mathrm{no}\,pump}}{W_p} \quad (6),$$

where $W_{s+i,\,pump}$ is the sum of the signal and idler energies in the presence of pump radiation, $W_{s,\,\mathrm{no}\,pump}$ is the initial signal energy, and W_p is the pump energy. This formula determines the fraction of the pump power that is converted to either the signal or idler wavelengths, i.e. the pump depletion.

Wavelength conversion was simulated in a 5-cm-long, 3-mm-thick LBO crystal. This crystal has the following advantages: high damage threshold (18.9 GW/cm^2), relatively high quadratic nonlinearity d_{eff} (0.85 pm/V), no spatial walk-off and large angular acceptance for the case of type-I noncritical phase-matching. Equation (4) suggests the use of longer crystals to achieve stable adiabatic conversion, 5 cm being the typical maximal length of commercially available samples. Moreover, there is another constraint on the maximal length of the crystal imposed by the temporal walk-off between the pump and signal pulses, which increases with distance. In fact, in the wavelength range we considered, the pulses would be separated by 1-1.5 ps after a propagation distance of 5 cm. As a consequence, longer crystals are not useful since the conversion between the interacting waves slows down as the pulses drift further apart in time while they propagate in the crystal.

To match theory with real-world applications, a maximal temperature gradient that suits both the crystal length and material properties was chosen. In a simple thermistor-based heating setup, we found that it is possible to maintain a temperature contrast of up to ~70° C in a 5 cm long crystal. For this temperature gradient and pump intensity below the damage threshold, condition (3) is satisfied for a ~200 nm wide signal wavelength range around 1400 nm. However, condition (4) is only loosely satisfied, since the difference in phase mismatches at the input and output of the crystal is smaller but comparable to the L/l^2 term for such a set of parameters.

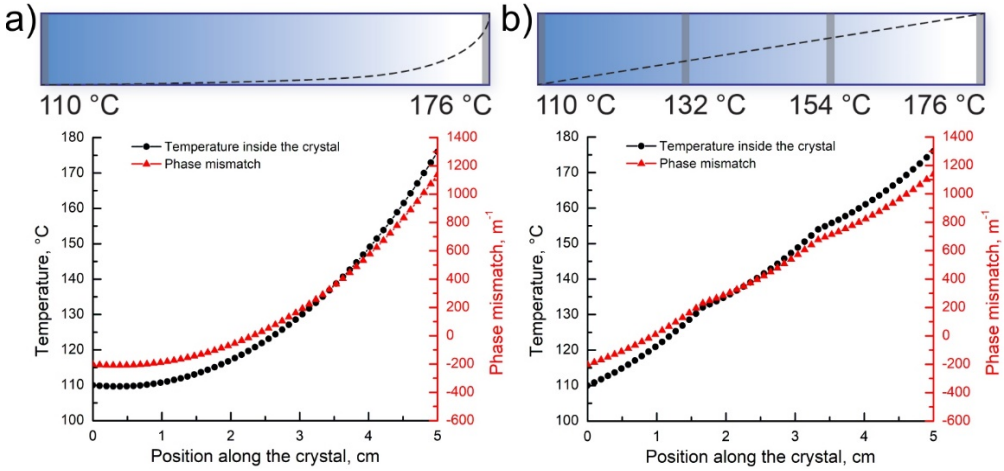

Fig. 1. Simulation of the temperature variation inside the crystal and the phase-mismatch as a function of the position in a 5-cm-long LBO crystal with $\lambda_3 = 775\,nm$ and $\lambda_2 = 1390\,nm$ for a) two heaters on the opposite sides of the crystal set to 110 and 176° C respectively, leading to an "exponential" temperature distribution and; b) four equidistant heaters along the crystal set to 110, 132, 154, and 176° C respectively, leading to a "linear" temperature distribution.

To tailor the temperature profile inside the crystal, we opted for either two or four heaters along its length. The outer surfaces of the crystal are allowed to exchange heat with the environment via convection; the heat transfer is proportional to the temperature difference between the crystal and the environment, with a coefficient of proportionality equal to 2

Optics EXPRESS

W/(m^2 K), as determined via experimental measurement of the temperature along the crystal length. The steady-state solution of the classical parabolic heat transfer equation:

$$\rho C\frac{\partial T}{\partial t}-\nabla\cdot\left(k\nabla T\right)=0 \qquad (7),$$

provides the temperature distribution inside the crystal where ρ is the LBO density, C is its specific heat, T is its temperature, and k is its thermal conductivity.

Figure 1(a) shows the numerically calculated temperature as a function of the horizontal position along the crystal when only two heaters on the opposite sides of the crystal were employed, and the temperatures on the left and right facets were stabilized at 110 and 176° C, respectively. For the given, 3-mm-thick crystal, the temperature gradient in the transverse plane is negligible. We call the resulting temperature distribution "exponential" throughout the text of the article. In the second case, the temperatures of the four equidistant points along the crystal were set to 110, 132, 154, and 176° C, respectively. The corresponding "linear" temperature distribution along with the phase-mismatch as a function of the position are presented in Fig. 1(b). Figure 1 also shows that the phase-mismatch between the three interacting waves is a virtually linear function of the temperature for a pump wavelength of $\lambda_3=775\,nm$ and a signal wavelength of $\lambda_2=1390\,nm$.

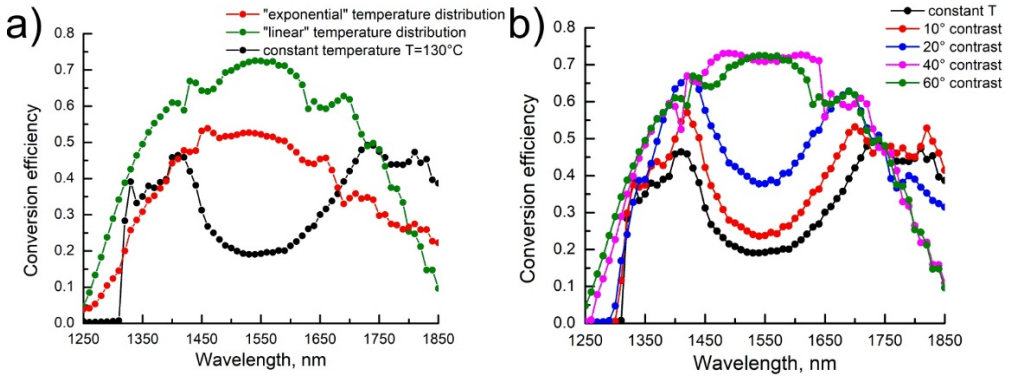

Fig. 2. a) Simulated conversion efficiency as a function of the wavelength for three temperature distributions inside the LBO crystal: exponential (red line) and linear (green line) temperature gradients with a contrast of 60 ° C, (100° C - 160° C) are compared to the constant temperature of 130 ° C (black line); b) Simulated conversion efficiency as a function of the wavelength for different linear temperature distributions inside the LBO crystal. Temperature contrasts between 40° C (110° C - 150° C) and 60° C (100° C - 160° C) feature the highest conversion efficiency and bandwidth.

To better understand the nature of adiabatic TWM, we have conducted a series of simulations to determine the optimal temperature distribution along the crystal. First, we compared the conversion efficiency from the pump at 775 nm to the signal varying from 1200 to 1850 nm for crystals featuring a constant temperature, as well as for two temperature distributions with exponential and linear gradients (see Fig. 1). For this analysis we used the following experimentally relevant parameters for the pump: Gaussian beam, 5 μJ energy, 0.19 mm width, 0.7 ps pulse duration; for the signal: Gaussian beam, 1 μJ energy, 0.19 mm width, 0.7 ps pulse duration. For the constant temperature case, we chose the value of 130 °C, since it yields perfect phase-matching for a pump $\lambda_3=775\,nm$ and a signal $\lambda_2=1390\,nm$ (at the center of the experimental signal bandwidth). Indeed, the calculations indicate that the TWM process is efficient for signal wavelengths of up to >1700 nm in non-uniform nonlinear crystals [see Fig. 2(a)]. Notably, the conversion efficiency in adiabatic non-uniform settings (i.e., linear and exponential profiles) is higher than for the uniform configuration over almost the entire examined wavelength range. An efficient (>45%) TWM conversion range of more

Optics EXPRESS

than 300 nm makes this scheme also suitable for the upconversion of ultrashort (~10 fs) femtosecond pulses. Note that for this application, the ultrashort pulse must be ideally stretched before the amplification to minimize the group velocity mismatch effect, and then recompressed after the crystal to recover the original pulse duration. For the same temperature contrast, a linear profile along the nonlinear crystal results in better performances of the TWM process compared to an exponential temperature distribution. In particular, a linear temperature distribution offers the most gradual phase mismatch change along the crystal [as required by Eq. (4)]. Consequently we observe, in this case, a higher and at the same time spectrally flatter conversion efficiency, compared to the exponential temperature gradient setting.

Furthermore, the temperature contrast for the linear gradient case can be optimized to achieve the best performances over a wide wavelength range. Figure 2(b) provides a comparison of the conversion efficiencies for different linear gradients centered at 130° C, showing a rapid improvement up to a temperature contrast of 40° C. Further increase does not result in a more efficient conversion or a wider phase-matching bandwidth.

4. Experiment

Based on the results of the simulations, we designed an experiment to verify the efficiency of the adiabatic parametric amplification. Figure 3 shows the schematic of the proposed setup, where a pump and signal wave were injected into the left facet of the crystal. We used an LBO crystal (Eksma Co., 3x3x50 mm, type 1, $\theta = 90°$, $\varphi = 0°$, uncoated), a 775 nm pump beam (up to 5 μJ of pulse energy, 0.7 ps duration, 6 nm spectral full width at half maximum), and a seed beam with wavelength tunable from 1200 to 1550 nm (pulse energy 1 μJ, 0.7 ps duration, 6 nm spectral full width at half maximum). While in the theoretical analysis the tuning range for the signal wave was not restricted, in the experiment it was limited by the output wavelength range of our commercial OPA, used to generate the seed wave.

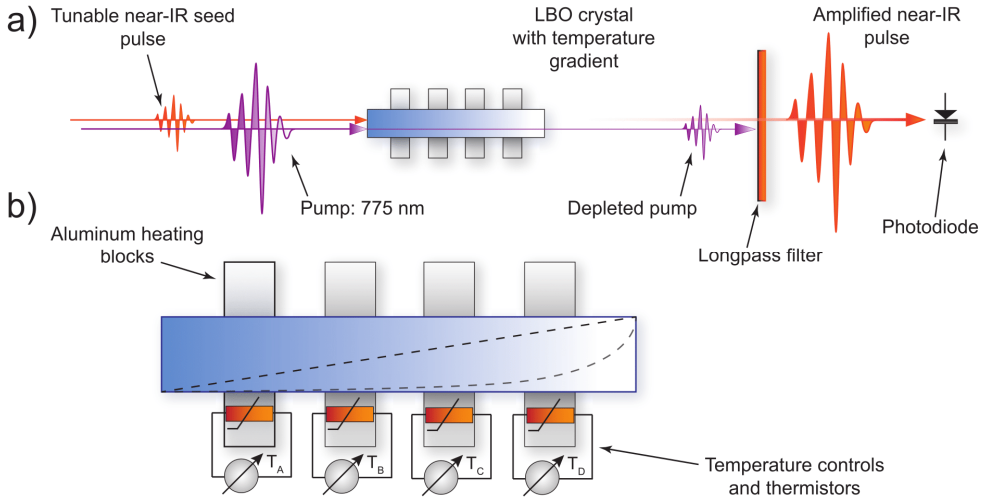

Fig. 3. a) Schematic of the experimental setup. A pump and signal waves are injected through the left facet of an LBO crystal with a temperature gradient applied along its length. Upon exiting the crystal, the pump wave is blocked by a longpass filter, whereas the amplified signal wave is detected via a photodiode. b) The temperature inside the crystal is controlled by heating four equidistantly-placed spots, using thermistors positioned in direct contact with the crystal surface.

A temperature contrast of up to 60° C was applied along the 5-cm-long LBO crystal to achieve the desired phase-matching conditions. A dichroic beamsplitter was used in order to combine the 775 nm pump and signal beams at the input of the crystal, while a 1000 nm longpass filter eliminated the 775 nm pump radiation after the crystal. A pyroelectric energy

Optics EXPRESS

meter (OPHIR PE9-SH) measured the signal power in the 1150-2000 nm wavelength range. We corrected for the frequency dependent response of the detector, as well as for the transmission of the longpass filter, which varied for the signal and idler wavelengths.

We constructed a crystal holder with built-in thermoelectric heaters. The temperature gradient inside the crystal was produced by heating four equidistantly-placed spots, respectively controlled by thermistors positioned in direct contact with the crystal surface [see Fig. 3]. In order to shield the detector from thermal radiation, the crystal was wrapped in an insulating mineral wool, and aluminum barriers were placed between the crystal and the detector. In this setup, it takes approximately 10 minutes for the 3-mm thick crystal to reach the required temperature distribution. By using even thicker (~10 mm) crystals, better optimized for high average power operation, the transition time to a steady thermal distribution will increase, however in that case the temperature inside the crystal can be more precisely controlled, since thicker crystals are less affected by convection. Note that the proposed technique does not require any complex fabrication or alignment techniques, making it practical for use in industrial grade optical parametric amplifiers.

Using this setup, we tested the three different types of temperature distributions previously simulated: i) uniform (four heaters set to the same temperature), ii) linear (four heaters whose temperatures formed an arithmetic progression), and iii) exponential temperature distribution (only two active heaters, at the crystal extremities). First, a temperature gradient of 60° C was imposed along the crystal to obtain adiabatic phase-matching conditions. We observed a peak conversion efficiency of 55% as well as a conversion bandwidth larger than 250 nm.

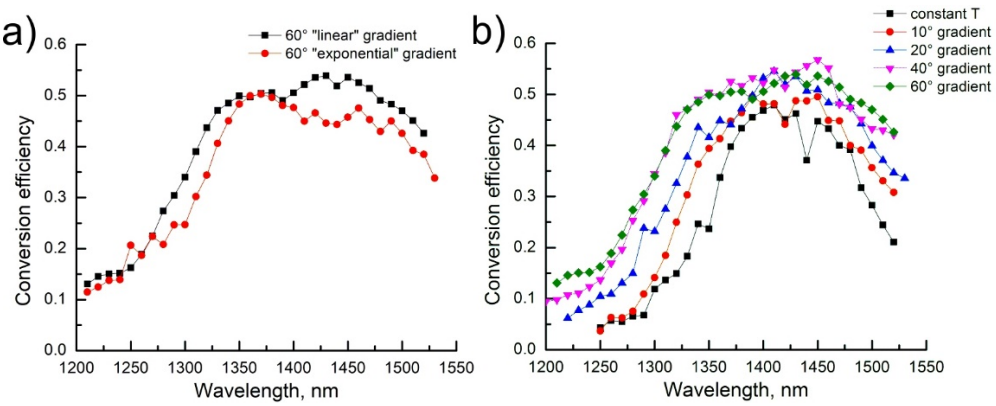

Fig. 4. a) Measured conversion efficiency as a function of the seed wavelength for the exponential and linear temperature gradients (centered around 130° C, with a contrast of 60° C); b) Measured conversion efficiency as a function of the seed wavelength for the linear temperature distributions (centered around 130° C, and with a varying temperature contrast).

Switching from an exponential temperature profile (only two active heaters at the ends of the crystal) to a linear profile (four active heaters) resulted in a 10% conversion efficiency increase and a broader bandwidth [see Fig. 4(a)]. Next, we characterized the conversion efficiency in the crystal for a uniform temperature of 130° C, and subsequently for varying gradients centered around the same temperature as above. Figure 4(b) shows a strong growth of the experimentally measured conversion efficiencies up to a temperature contrast of 40° C. As predicted by our numerical results, extending the contrast beyond this point (up to 60° C) did not result in a broader phase-matching bandwidth or a higher conversion efficiency.

The conversion efficiency demonstrated in the experiment is ~10% lower than that predicted by the numerical simulations. We attribute this difference to imprecision in the control of the crystal temperature using our heating system. Indeed, the thermoelectric heaters have dimensions on the order of several mm, thus there is no variation in temperature on the

Optics EXPRESS

parts of the crystal directly touching a particular heater, whereas a temperature gradient is only applied between consecutive heaters. Therefore, there is potential for improving the conversion efficiency by using a larger amount of smaller heating elements towards obtaining the desired temperature profile with higher precision.

5. Conclusion

In this work, we have studied TWM in the adiabatic regime within a bulk non-uniform nonlinear crystal. We have demonstrated that the wave vector mismatch can be controlled by inducing a suitable temperature gradient along the crystal length. We have shown that a linear temperature profile inside the crystal resulted in an almost flat conversion efficiency >50% over a wide ~250 nm spectral bandwidth. We believe that the demonstrated technique not only proves, from a fundamental point of view, the universality of the autoresonance principle, but also paves the way to a new generation of OPAs. Furthermore, it can be readily applied to existing OPA setups, since it does not require any changes other than applying a temperature distribution along the nonlinear crystal. Our simple scheme allows for quick reconfiguration, as the same crystal can be used to meet phase-matching conditions in different wavelength ranges. In addition to, e.g., the amplification of continuum sources for spectroscopy and in contrast to other approaches (including periodic-poling), our technique can be extended to high power applications, such as the generation of ultrabroadband few-cycle pulses for attosecond science. Opportunities to further increase both the bandwidth and efficiency of our conversion scheme will rely on a more precise control over the crystal temperature distribution, which may also yield a smoother and customizable amplification spectrum.

Funding

Strategic and Discovery Grants Schemes (NSERC); Canada Research Chair Program; MESI PSR-SIIRI Initiative; ITMO Fellowship and Professorship Program (074-U01); 1000 Talents Sichuan Program (R.M.); Engineering and Physical Sciences Research Council (EPSRC, Grants No. EP/P009697/1 and EP/R511705/1).

Comment

All relevant data present in this publication can be accessed at: http://dx.doi.org/10.5525/gla.researchdata.576.